doi:10.1246/cl.2011.46

Published on the web November 25, 2010

# Expansion of Intertubular Mesopores of Imogolite Nanotubes by Thermal Decomposition of an Imogolite–Poly(sodium 4-styrenesulfonate) Composite

Yoshiyuki Kuroda[1] and Kazuyuki Kuroda*[1,2]
[1]*Department of Applied Chemistry, Faculty of Science and Engineering, Waseda University, 3-4-1 Ohkubo, Shinjuku-ku, Tokyo 169-8555*
[2]*Kagami Memorial Research Institute for Materials Science and Technology, Waseda University, 2-8-26 Nishiwaseda, Shinjuku-ku, Tokyo 169-0051*

(Received October 18, 2010; CL-100886; E-mail: kuroda@waseda.jp)

Intertubular mesopores of imogolite nanotubes were enlarged by using poly(sodium 4-styrenesulfonate) as an expander. The polyanion was bound electrostatically on the positively charged imogolite nanotubes to form an intertwined composite, which provided expanded intertubular mesopores after heat treatment. The expanded intertubular mesopores are expected to contribute to efficient diffusion.

Imogolite is a naturally occurring aluminosilicate nanotube, whose general composition is $Al_2SiO_3(OH)_4$, with a unique structure.[1] The inner and outer diameters of imogolite are ca. 1 and ca. 2 nm, respectively. The inner and outer surfaces are covered with SiOH and AlOH groups, respectively, enabling surface modification.[2] Imogolite is promising as an adsorbent,[3] heat-exchange material,[4] catalyst,[5] and catalyst support,[6] because of its uniform intratubular micropores. Imogolite also possesses mesopores among bundles consisting of 3 or 4 parallel nanotubes[7] (intertubular mesopores). The rate of water vapor adsorption on imogolite faster than on zeolites and silica gel is explained by the presence of the intertubular mesopores.[4] However, the size of intertubular mesopores are usually small because most of them are formed among closely packed and oriented bundles (Scheme 1). Therefore, the control of intertubular mesopores is promising to improve the efficiency of diffusion for some of the applications listed above. We have reported macroporous materials whose pore walls consist of imogolite nanotubes, whereas the walls collapse under thermal or hydrothermal conditions when walls are too thin.[8] It is important to expand intertubular mesopores in robust aggregates of imogolite.

To expand the intertubular mesopores, the insertion of additives among nanotubes or bundles is promising. Utsumi, Kaneko, et al. have reported the insertion of $C_{60}$ among single-wall carbon nanotubes (SWNT) and their enhanced adsorption capacity for $H_2$.[9] However, the surface properties of imogolite are quite different from that of SWNT. We then focused on poly(4-styrenesulfonate) (PSS) anion that is bound electrostatically on the outer surface of imogolite which is cationic by adsorbing $H^+$ on the outer AlOH groups.[10] We[8b] and Takahara et al.[11] have reported layer-by-layer assemblies of imogolite and polyanions, the method of which means that excess polyanions are excluded due to their electrostatic repulsion. Thus, a uniform structural change is expected, even in random aggregates of polydisperse imogolite nanotubes.

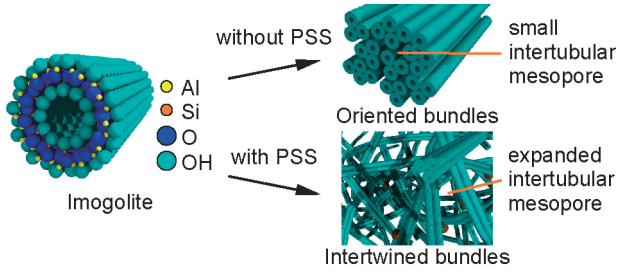


**Scheme 1.** Illustration of the packing structures of imogolite bundles.

In this paper, we demonstrate the expansion of intertubular mesopores of imogolite by thermal decomposition of an imogolite–PSS composite. PSS is adsorbed on the outer surface of imogolite, which is expected to provide a randomly intertwined composite (Scheme 1). Expanded intertubular mesopores are formed after heat treatment of the composite.

Imogolite was synthesized according to the literature.[12–14] The concentration of imogolite sol was adjusted to ca. 1 mg mL$^{-1}$. A solution (2 mL) containing 100 mg mL$^{-1}$ PSSNa ($M_w = 70000$, Sigma-Aldrich Co.) was added slowly (ca. 0.2 mL min$^{-1}$) into the sol (200 mL) under vigorous stirring. The mixture of the sol and PSS finally gelled together to form transparent hydrogel. The hydrogel was then washed with water and centrifuged three times. After being dried at 80 °C, a slightly yellow powdery imogolite–PSS composite was obtained. Imogolite and the composite were further heat-treated at 400 °C for 3 h under ambient conditions (denoted as heat-treated imogolite and heat-treated composite, respectively).

Fourier transform infrared (FTIR) spectra were recorded on a Perkin-Elmer Spectrum One spectrometer using a KBr disc. X-ray diffraction (XRD) patterns were obtained by a Rigaku Ultima-III diffractometer using Cu K$\alpha$ radiation (40 kV, 40 mA). Carbon contents were determined by CHN analysis using a Perkin-Elmer PE-2400II apparatus. Thermogravimetry–differential thermal analysis (TG–DTA) curves were recorded on a Rigaku TG8020 instrument with a heating rate of 10 °C min$^{-1}$ under a dry air flow. High-resolution scanning electron microscope (HRSEM) images were obtained by a Hitachi S-5500 microscopy with accelerating voltage at 1 kV. EDX spectra were recorded on a JEOL JED-2300T spectrometer. The samples were observed without metal coating. $N_2$ adsorption–desorption isotherms were measured by a Quantachrome Autosorb-1 apparatus. The samples were degassed at 120 °C for 24 h prior to the measurement. The pore size distribution histograms were calculated by the nonlocalized density functional theory (NLDFT) using the adsorption branches.

The FTIR spectrum of imogolite shows a sharp peak at 1384 cm$^{-1}$ due to the stretching vibration of $NO_3^-$ which is a

  

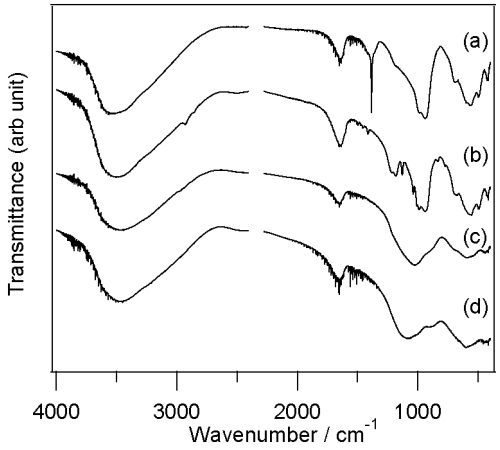


**Figure 1.** FTIR spectra of (a) imogolite, (b) imogolite–PSS composite, (c) heat-treated imogolite, and (d) the heat-treated composite.

counter anion of $AlOH_2^+$ on the outer surface (Figure 1a). The peak disappeared in the spectrum of the imogolite–PSS composite (Figure 1b), and the bands due to PSS appeared (the spectra and the assignments of imogolite and PSS sodium salt are shown in the Supporting Information, Figure S1[15]). The absence of Na in the imogolite–PSS composite was also confirmed by the EDX analysis (data not shown). Therefore, PSS interacts directly with imogolite by replacement with $NO_3^-$. Because the composite formed hydrogels, PSS anions probably bridged among bundles of imogolite to form a randomly intertwined structure.

The broad peaks observed in the low-angle XRD patterns of imogolite and the imogolite–PSS composite are mainly due to their bundled structures (Figure 2). Jones, Nair, et al. have investigated the origin of the broad peaks by simulations of the XRD patterns.[7] The broadness of the peaks indicates that a bundle consists of 3 or 4 nanotubes without long-range ordering. Though bundles are parallelly packed, the arrangement of the nanotubes is not coherent. Because broad low-angle peaks are observed in the XRD pattern of imogolite–PSS, the composite also possesses bundled structure. PSS anions are probably adsorbed on the outer surface of bundles. Moreover, a new shoulder peak appeared at ca. 2° ($d$ = ca. 4 nm, indicated with an asterisk in Figure 2b). The shoulder may be attributed to a small amount of parallel assembly of nanotubes coated individually with PSS.

The FTIR spectra of heat-treated imogolite and the heat-treated composite show the shifts of the absorption bands due to the Si–O–Al stretching vibrations from 940 and 990 $cm^{-1}$ to 1030 $cm^{-1}$, which indicates dehydroxylation of imogolite (Figures 1c and 1d).[7,16] The wide-angle XRD patterns of heat-treated imogolite and the heat-treated composite show their amorphous structures (Figure S2[15]). Although the crystal structure of imogolite collapsed by heat treatment, we have previously confirmed that intratubular micropores are largely retained.[8]

After heat treatment, the composite turned brown, whereas heat-treated imogolite is white. The brown color is due to carbonaceous residue provided by incomplete combustion of PSS. The carbon content of the heat-treated composite was

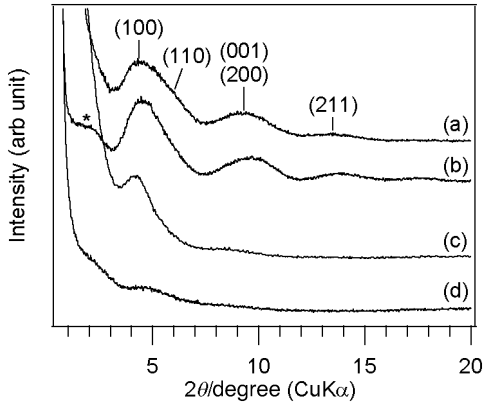


**Figure 2.** XRD patterns of (a) imogolite, (b) imogolite–PSS composite, (c) heat-treated imogolite, and (d) the heat-treated composite.

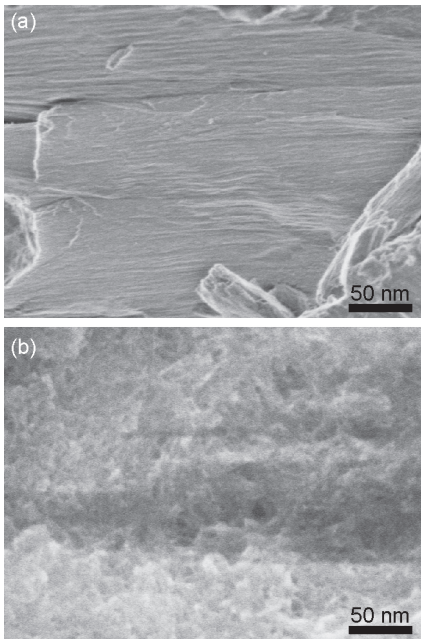


**Figure 3.** HRSEM images of (a) heat-treated imogolite and (b) the heat-treated composite.

7.0%. The TG–DTA curves of imogolite–PSS composite indicate ca. 24% mass loss at 400 °C (Figure S3[15]). Because the PSS content in the composite is estimated to be ca. 25 wt % by CHN analysis, the amount of residue is calculated to be ca. 9 wt %,[17] in which 7 wt % of carbonaceous materials and ca. 2 wt % of sulfate residue may be included. The weak bands at 609 and 1090 $cm^{-1}$ in the FTIR spectrum of the heat-treated composite can be attributed to sulfate (Figure 1d).[18]

The HRSEM image of heat-treated imogolite shows parallel-oriented imogolite bundles (Figure 3a), whereas that of the heat-treated composite shows intertwined bundles (Figure 3b). Their high-magnification images are shown in Figure S4.[15] The low-angle XRD pattern of the heat-treated composite suggests the deformation of the bundled structure, while such a deformation of imogolite is not so noticeable (Figures 2c and 2d). Because the bundles of imogolite without

  

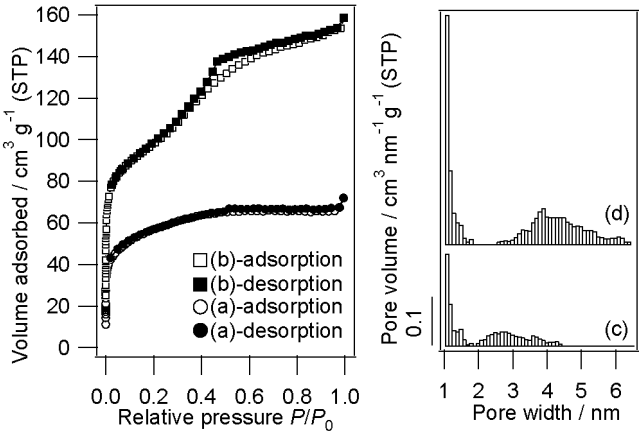


**Figure 4.** $N_2$ adsorption–desorption isotherms of (a) heat-treated imogolite and (b) the heat-treated composite, and (c, d) their NLDFT pore size distribution histograms, respectively.

PSS are highly oriented, it is reasonable that some imogolite nanotubes rearrange into an ordered packing. Contrary, the randomly intertwined bundles of imogolite–PSS composite are probably difficult to rearrange into an ordered packing.

The $N_2$ adsorption–desorption isotherm of heat-treated imogolite corresponds to a type I curve (Figure 4a), whereas that of the heat-treated composite shows a type IV curve with an obvious uptake at $P/P_0 = 0.3$–$0.5$ (Figure 4b). Such a capillary condensation is not observed usually for imogolite with random mesopores. The pore size distribution histograms, determined by NLDFT, also show the presence of *intra*tubular micropores and *inter*tubular mesopores for both (Figures 4c and 4d). The sizes of intratubular micropores are almost the same, whereas the intertubular mesopore of the heat-treated composite is larger (3–6 nm) than that of heat-treated imogolite (2–4 nm). Moreover, the total pore volume is increased from 0.11 to 0.26 $cm^3 g^{-1}$, which is consistent with its structure. The micropore volume was also increased, which is possibly due to the formation of micropores among bundles or the improved accessibility of intratubular micropores. The BET surface areas of heat-treated imogolite and the heat-treated composite are 209 and 355 $m^2 g^{-1}$, respectively. These changes show the improved accessibility of the heat-treated composite. This surface area is not the highest among those of heat-treated imogolite aggregates,[3] because the tubular structure of the present imogolite partially collapsed due to the heat treatment.[7,17] However, the expansion shown here is meaningful because heat treatment is necessary in many cases when organic templates are used.[8]

The expansion of the intertubular mesopores is probably explained by randomly intertwined bundles in an immediately formed aggregate. Enlarged distance among imogolite nanotubes is retained after the removal of PSS. In our previous report on the layer-by-layer assembly of imogolite and PSS,[8b,19] well-defined capillary condensation due to expanded mesopores was not observed. Stacked layers composed of imogolite and PSS were formed, in which PSS did not penetrate into the intertubular mesopores of imogolite. Therefore, the randomly intertwined structure formed in the homogeneous dispersion used in this study is thought to be important for the intertubular expansion.

In conclusion, intertubular mesopores of imogolite nanotubes are expanded by using PSS as an expander. Imogolite bundles are randomly intertwined to show larger pore size and higher surface area than those of heat-treated imogolite. The present method contributes extensively to the applications using imogolite as adsorbents with efficient diffusion.

This work was supported by the Elements Science and Technology Project "Functional Designs of Silicon-Oxygen-Based Compounds by Precise Synthetic Strategies" and the Global COE program "Practical Chemical Wisdom" from MEXT, Japan. The A3 Foresight Program "Synthesis and Structural Resolution of Novel Mesoporous Materials" supported by the Japan Society for the Promotion of Science (JSPS) is also acknowledged. Y. K. is grateful for financial support via a Grant-in-Aid for JSPS Fellows from MEXT.

## References and Notes

1 P. D. G. Cradwick, V. C. Farmer, J. D. Russel, C. R. Masson, K. Wada, N. Yoshinaga, *Nature (London), Phys. Sci.* **1972**, *240*, 187.
2 a) L. M. Johnson, T. J. Pinnavaia, *Langmuir* **1991**, *7*, 2636. b) K. Yamamoto, H. Otsuka, A. Takahara, *Polym. J.* **2007**, *39*, 1.
3 W. C. Ackerman, D. M. Smith, J. C. Huling, Y.-W. Kim, J. K. Bailey, C. J. Brinker, *Langmuir* **1993**, *9*, 1051.
4 a) M. Suzuki, K. Inukai, *Top. Appl. Phys.* **2010**, *117*, 159. b) M. Suzuki, S. Suzuki, M. Maeda, S. Tomura, T. Mizota, *J. Ceram. Soc. Jpn.* **2001**, *109*, 874.
5 M. Ookawa, Y. Takata, M. Suzuki, K. Inukai, T. Maekawa, T. Yamaguchi, *Res. Chem. Intermed.* **2008**, *34*, 679.
6 S. Imamura, T. Kokubu, T. Yamashita, Y. Okamoto, K. Kajiwara, H. Kanai, *J. Catal.* **1996**, *160*, 137.
7 D.-Y. Kang, J. Zang, E. R. Wright, A. L. McCanna, C. W. Jones, S. Nair, *ACS Nano* **2010**, *4*, 4897.
8 a) Y. Kuroda, M. Tamakoshi, J. Murakami, K. Kuroda, *J. Ceram. Soc. Jpn.* **2007**, *115*, 233. b) Y. Kuroda, K. Kuroda, *Sci. Technol. Adv. Mater.* **2008**, *9*, 025018.
9 M. Arai, S. Utsumi, M. Kanamaru, K. Urita, T. Fujimori, N. Yoshizawa, D. Noguchi, K. Nishiyama, Y. Hattori, F. Okino, T. Ohba, H. Tanaka, H. Kanoh, K. Kaneko, *Nano Lett.* **2009**, *9*, 3694.
10 Y. Horikawa, *Clay Sci.* **1975**, *4*, 255.
11 N. Jiravanichanun, K. Yamamoto, H. Yonemura, S. Yamada, H. Otsuka, A. Takahara, *Bull. Chem. Soc. Jpn.* **2008**, *81*, 1663.
12 V. C. Farmer, M. J. Adams, A. R. Fraser, F. Palmieri, *Clay Miner.* **1983**, *18*, 459.
13 S.-I. Wada, *Nendo Kagaku* **1985**, *25*, 53.
14 M. Suzuki, F. Ohashi, K. Inukai, M. Maeda, S. Tomura, *Nendo Kagaku* **2000**, *40*, 1.
15 Supporting Information is available electronically on the CSJ-Journal Web site, http://www.csj.jp/journals/chem-lett/index.html.
16 J. D. Russell, W. J. McHardy, A. R. Fraser, *Clay Miner.* **1969**, *8*, 87.
17 The mass loss of the composite (ca. 24 wt %) is explained as the sum of dehydroxylation of imogolite (ca. 8 wt %) and decomposition of PSS (ca. 16 wt %), because imogolite usually loses ca. 10 wt % of its mass at 300–400 °C. Therefore, the residue of PSS is calculated to be ca. 9 wt %.
18 G. Socrates, *Infrared and Raman Characteristic Group Frequencies: Tables and Charts*, 3rd ed., Wiley, New York, **2004**.
19 Y. Kuroda, K. Kuroda, *Bull. Chem. Soc. Jpn.* **2011**, *84*, in press.

  